Supporting Information

Oxygen Vacancy Induced Room Temperature Metal-Insulator Transition in Nickelate Films and Its Potential Application in Photovoltaics

Le Wang,[†] Sibashisa Dash,[†] Lei Chang,[†] Lu You,[†] Yaqing Feng,[‡] Xu He,[‡] Kui-juan Jin,[‡,§] Yang Zhou,[†] Hock Guan Ong,[∥] Peng Ren,[†] Shiwei Wang,[†] Lang Chen,[⊥] and Junling Wang[*,†]

[†]School of Materials Science and Engineering, Nanyang Technological University, 639798, Singapore

[‡]Institute of Physics, Chinese Academy of Sciences, Beijing 100190, China

[§]Collaborative Innovation Center of Quantum Matter, Beijing, 100190, China

[∥]Temasek Laboratories@NTU, Nanyang Technological University, 637553, Singapore

[⊥]Department of Physics, South University of Science and Technology of China, Shen Zhen, 518055, China

[*]Email: jlwang@ntu.edu.sg

Film thickness plays an important role in the properties of $RNiO_3$ films.[1-4] As shown in Figure S1a, all of the as-grown NNO films show metallic behavior at room temperature. Figure S1b shows the room temperature R_{sheet} change after annealing as a function of NNO film thickness. The room temperature R_{sheet} of 10 u.c. NNO film increases by six orders of magnitude after being annealed at 180 ℃ for 20 minutes. With further annealing at higher temperature, R_{sheet} gradually saturates. For the thickest NNO film, although the room temperature metallic behavior is changed to insulating behavior after annealing in vacuum at 300 ℃, only two orders of magnitude modulation in R_{sheet} at room temperature was observed. Moreover, after annealing in O_2 environment at 300 ℃, all of the NNO films recover the as-grown metallic state. It can be seen that the change of sheet resistance (ΔR_{sheet}) between the as-grown state and after annealing in vacuum becomes larger with increasing vacuum annealing temperature. On the other hand, ΔR_{sheet} becomes smaller with increasing film thickness, indicating that oxygen vacancies are more likely created in thinner films.

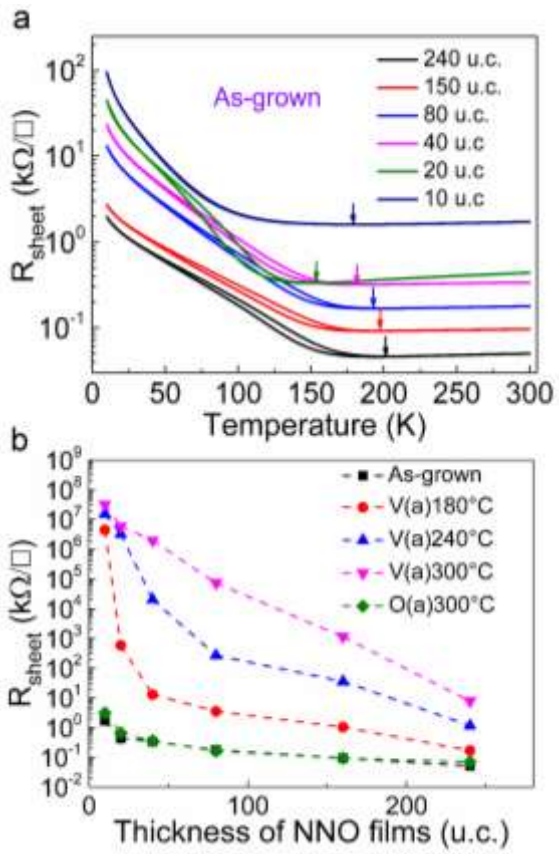

Figure S1. Thickness effect on the oxygen vacancy induced insulating phase. (**a**) R_{sheet} versus temperature curves for $NdNiO_3$ (NNO) films of various thickness grown on STO. The arrows show the metal insulator transition temperature (T_{MI}) upon heating. (**b**) The effect of NNO film thickness on the room temperature R_{sheet} change induced by oxygen vacancies.

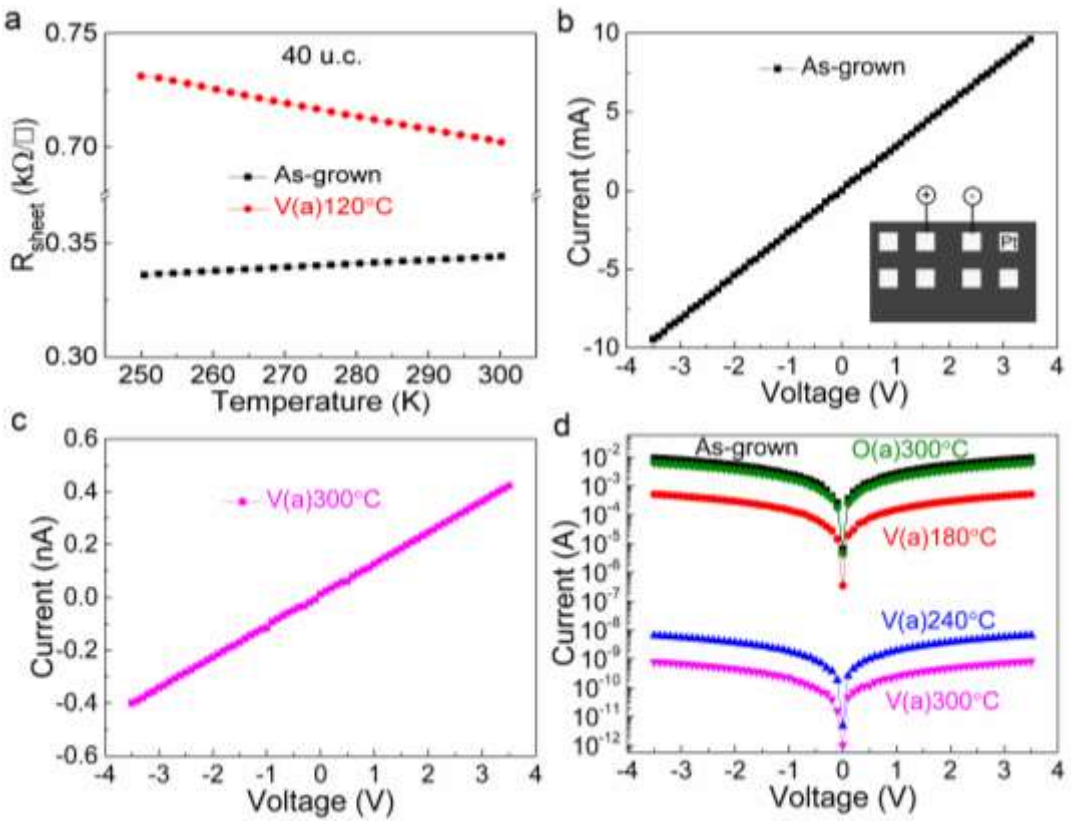

Figure S2. Ohmic contact. (**a**) R_{sheet} versus temperature for 40 u.c. NNO films at the as-grown state and after vacuum annealing at 120 ℃ for 20 min. Clear metal-insulator transition is observed. (**b**) I-V curve of as-grown 40 u.c NNO film. The inset shows the schematic diagram for I-V measurements. (**c**) I-V curve of 40 u.c thick NNO film at the state of V(a)300℃. The good linear relationship indicates the Ohmic contact between Pt and NNO. (**d**) Logarithmic I-V characteristics for the NNO films at various states.

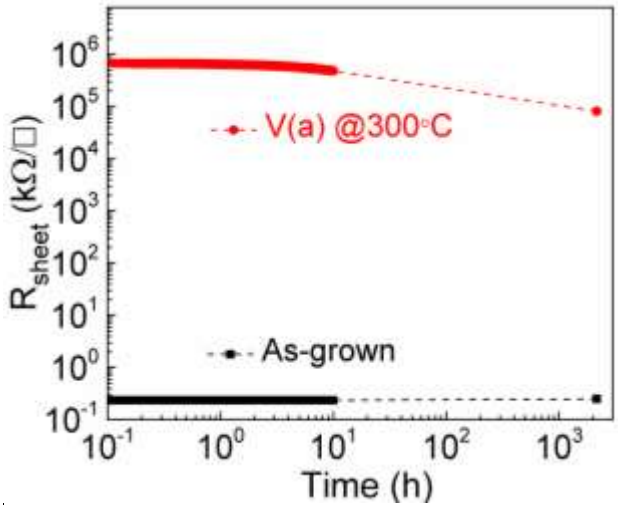

Figure S3. Retention characteristic of the NNO films at room temperature. The black squares correspond to the R_{sheet} of as-grown film, while the red circles correspond to the R_{sheet} of V(a)300℃ film. Only one order of magnitude decay in the R_{sheet} is observed after three months.

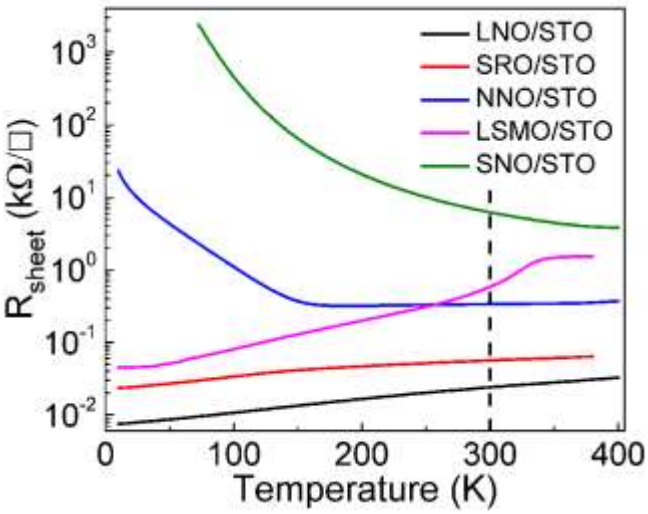

Figure S4. Comparison with other widely studied oxides. R_{sheet} versus temperature curves for the as-grown $LaNiO_3$ (LNO), $SrRuO_3$ (SRO), NNO, $La_{0.7}Sr_{0.3}MnO_3$ (LSMO) and $SmNiO_3$ (SNO) films grown on STO substrate. The dash line shows the difference of their R_{sheet} values at room temperature.

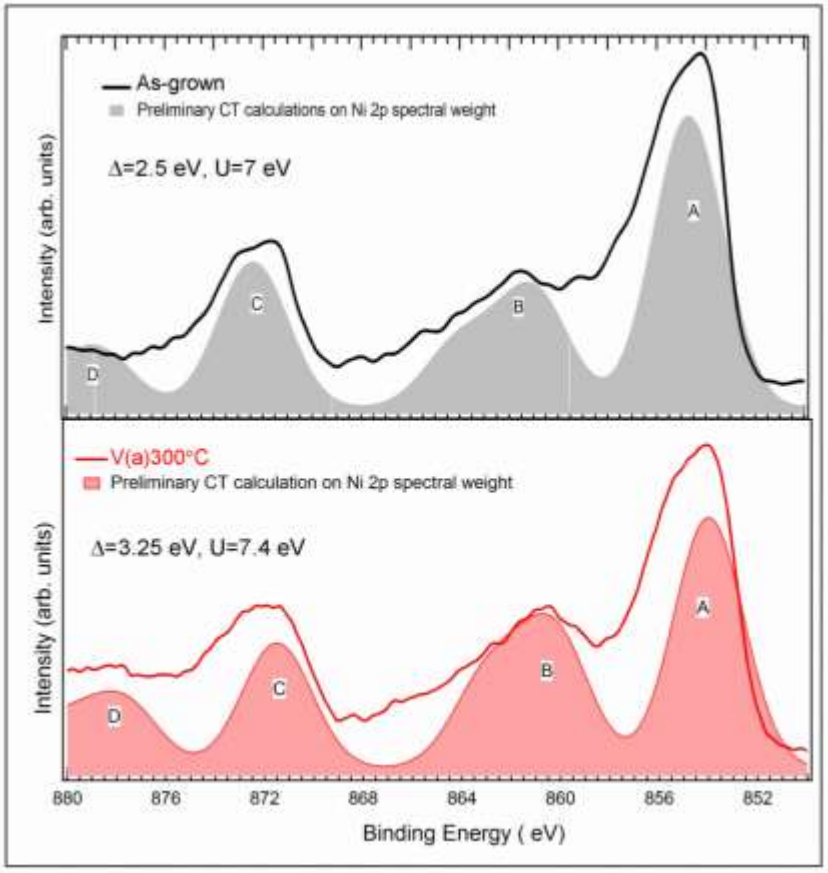

Figure S5. Preliminary charge transfer calculation based on XPS results. The Ni 2p XPS spectra containing peaks A and C due to spin orbit splitting and their satellite peaks B and D are shown in Figure S5. Satellites are often found in Ni based oxides and are ascribed to charge transfer (CT) effects from the ligand anions (O 2p) to the Ni 3d levels. These effects can be accounted for in the frame of a configuration interaction (CI) model, where the electronic states involved in the photoemission process are described by a linear combination of several configurations such as $3d^n$, $3d^{n+1}\underline{L}$, $3d^{n+2}\underline{L}^2$ ($\underline{L}$ represents a hole in the anion created by the CT to the *3d* cation orbitals).[5] The CT energy (Δ) is defined by $=E(d^{n+1})-E(d^n)$. The positions of B and D satellites vary depending on Δ between the *p* and *d* orbitals involved in the CT process (here from O *2p* to Ni *3d*). U is the on-site coulomb repulsion between *d* electrons and Q_{pd} is the intra-atomic coulomb interaction between *p* and *d* orbitals. CT calculation is applied to Ni *2p* spectra for as-

grown and vacuum annealed samples, as shown in Figure S5. In fact, CT calculation was also reported on other transition metal systems, such as the Mn:Ge(111) interfaces.[6] For the case of as-grown sample, the calculated CT (shaded area) curve (upper panel in Figure S5) is obtained with Δ =2.5 eV, U = 7 eV, and Q_{pd} = 9 eV. Calculated CT curve (shaded area) for the sample with the state of V(a)300℃ has been obtained (lower panel in Figure S5) by setting Δ =3.25 eV, U = 7.4 eV, and Q_{pd} =10.6 eV. These findings are consistent with those obtained on NiO systems.[7,8] Δ, U, Q_{pd} for the insulating state (vacuum annealed sample) is 0.75, 0.4 and 1.6 eV higher than the metallic state (as-grown sample) and it roughly scales the gap and hence discriminates the two systems. In addition to this, the spin orbit split of as-grown sample (17.7 eV) is quenched to 17.5 eV for the sample with the state of V(a)300℃, as a signature of transition to Ni^{2+} of NiO-like system.

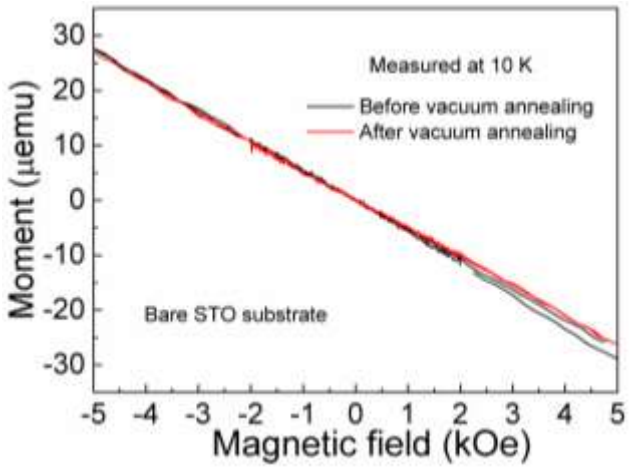

Figure S6. Diamagnetism of the bare STO substrates. We have also measured the magnetic properties of the bare STO substrate. No obvious change in the magnetic properties has been observed before and after the annealing process (at 300℃), as shown in the following Figure S6. Therefore, the possible contribution from the substrate to the change of the magnetic properties can be ruled out in our work.

References

(1) Catalan, G.; Bowman, R.; Gregg, J. Metal-Insulator Transitions in $NdNiO_3$ Thin Films. *Phys. Rev. B* **2000**, 62 7892.

(2) Scherwitzl, R.; Gariglio, S.; Gabay, M.; Zubko, P.; Gibert, M.; Triscone, J.-M. Metal-Insulator Transition in Ultrathin $LaNiO_3$ Films. *Phys. Rev. Lett.* **2011**, 106, 246403.

(3) Scherwitzl, R.; Zubko, P.; Lezama, I. G.; Ono, S.; Morpurgo, A. F.; Catalan, G.; Triscone, J. M. Electric-Field Control of the Metal-Insulator Transition in Ultrathin $NdNiO_3$ Films. *Adv. Mater.* **2010**, 22, 5517-5520.

(4) King, P. D. C.; Wei, H. I.; Nie, Y. F.; Uchida, M.; Adamo, C.; Zhu, S.; He, X.; Božović, I.; Schlom, D. G.; Shen, K. M. Atomic-Scale Control of Competing Electronic Phases in Ultrathin $LaNiO_3$. *Nat. Nanotechnol.* **2014**, 9, 443–447.

(5) Okabayashi, J.; Kimura, A.; Rader, O.; Mizokawa, T.; Fujimori, A.; Hayashi, T.; Tanaka, M. Core-Level Photoemission Study of Ga1− xMnxAs. *Phys. Rev. B* **1998**, 58, R4211.

(6) Dash, S.; Mozzati, M. C.; Galinetto, P.; Drera, G.; Pagliara, S.; Sangaletti, L. Magnetism and Electronic Properties of Mn:Ge(111) Interfaces Probed by Core Level Photoemission Spectroscopy. *J. Phys.: Conf. Ser.* **2012**, 391, 012088.

(7) Bocquet, A.; Mizokawa, T.; Saitoh, T.; Namatame, H.; Fujimori, A. Electronic Structure of 3d-Transition-Metal Compounds by Analysis of the 2p Core-Level Photoemission Spectra. *Phys. Rev. B* **1992**, 46, 3771.

(8) Mizokawa, T.; Fujimori, A. Unrestricted Hartree-Fock Study of Transition-Metal Oxides: Spin and Orbital Ordering in Perovskite-Type Lattice. *Phys. Rev. B* **1995**, 51, 12880.